A NEW DECONVOLUTION METHOD FOR ANALYSIS OF PROBABILITY DENSITY DISTRIBUTION SPECTRA OBSERVED IN GAMMA-RAY INTERROGATION MEASUREMENTS OF MULTI-PHASE FLOWS

D.D.S. Liu

ENERGY RESEARCH PROGRAM
ENERGY RESEARCH LABORATORIES

CANMET REPORT 85-8E

NOVEMBER 1984

Available in Canada through

Authorized Bookstore Agents
and other bookstores

or by mail from

Canadian Government Publishing Centre
Supply and Services Canada
Ottawa, Canada K1A 0S9

Catalogue No. M 38-13/85-8E
ISBN 0-660-12033-X

Canada: $4.25
Other Countries: $5.10

Price subject to change without notice

A New Deconvolution Method for Analysis of Probability Density Distribution Spectra Observed in Gamma-Ray Interrogation Measurements of Multi-Phase Flows

*D.D.S. Liu**

Abstract

A numerical method for the deconvolution of probability density distribution spectra (PDDS) has been developed. It is based on principles of the least square and the Newton-Raphson iteration algorithm. The PDDS were obtained from measurements of multi-phase flows using a gamma-ray interrogation technique developed recently in the Synthetic Fuels Research Laboratory of the Energy Research Laboratories, CANMET in collaboration with the Chalk River Nuclear Laboratories, Atomic Energy of Canada Limited. The deconvoluted PDDS contain information on the hydrodynamic parameters of multi-phase flow phenomena.

Fundamental equations for the numerical method were translated into a Fortran program for practical applications. Examples of PDDS deconvolutions for both simulated and observed spectra are given.

*Research Scientist, Synthetic Fuels Research Laboratory, Energy Research Laboratories, CANMET, Energy, Mines and Resources Canada, Ottawa, K1A 0G1.

Nouvelle méthode de déconvolution pour l'analyse des spectres de distribution de la densité de probabilité obtenus lors de mesures d'interrogation aux rayons gamma d'écoulements multiphases

*D.D.S. Liu**

Résumé

Une méthode numérique de déconvolution des spectres de distribution de la densité de probabilité (SDDP) a été élaborée. Elle est basée sur les principes des moindres carrés et sur l'algorithme d'itération de Newton-Raphson. Les SDDP ont été obtenus lors de mesures d'écoulements multiphases basées sur une technique d'interrogation aux rayons gamma récemment mise au point au Laboratoire de recherche sur les combustibles synthétiques des Laboratoires de recherche sur l'énergie (CANMET), en collaboration avec les laboratoires nucléaires de Chalk River d'Energie atomique du Canada, Limitée. La déconvolution des SDDP fournit des renseignements sur les paramètres hydrodynamiques des phénomènes d'écoulement multiphase.

Un programme Fortran contenant les équations fondamentales utilisées dans la méthode numérique a été écrit en vue d'applications pratiques. Des exemples de déconvolution de SDDP simulés et observés sont donnés.

*Chercheur, Laboratoire de recherche sur les combustibles synthétiques, Laboratoires de recherche sur l'énergie, CANMET, Énergie, Mines et Ressources Canada, Ottawa, K1A 0G1.

CONTENTS

TABLES

FIGURES

INTRODUCTION

Bubble columns are widely used as absorbers, catalytic slurry reactors, and bioreactors (1-5). Although easy to use, bubble columns are difficult to design because their multi-phase flow characteristics are complex. Hydrodynamic studies of multi-phase flows at low temperatures and pressures can be easily carried out using instruments described in the literature (6-9). At high temperatures and pressures, however, difficulties occur because the instruments cannot be immersed suitably in the flow, creating a need for signals which can penetrate the thick reactor walls.

The gamma-ray interrogation method, developed by CANMET in collaboration with the Atomic Energy of Canada Limited's Chalk River Nuclear Laboratories (AECL-CRNL), offers an excellent option (10). No insertion of probes is required.

The principle of gamma-ray interrogation technique for multi-phase flow measurements and statistical methods for data analyses was described previously (10). It shows that the probability density distribution spectra (PDDS) can be used to derive information on factors such as time-averaged holdups, homogeneity of flow fields, bubble size distributions, and flow regimes.

Because of the random emission of photons from a radioisotope, the detected signal fluctuates randomly about a mean value. In a homogeneous flow field, the observed PDDS would be a Poisson distribution with a natural standard deviation (Fig. 1). In this case, the mean counting rate is directly related to the mean path length of gamma-rays passing through the material being measured.

However, in most measurements of multi-phase flow carried out in the present work, the PDDS appear highly asymmetrical (Figs. 2 to 4). Accordingly, not only is the mean counting rate important, but also the shape of the PDD spectrum including major peaks and shoulders must be considered in order to obtain information on hydrodynamic behaviour (11).

To obtain detailed information, a statistical model was developed (11). It involves the deconvolution of PDDS. A numerical method for deconvolution of PDDS for use in analyzing the hydrodynamic behaviour with the model is described.

THEORY

Convolution and Deconvolution

Consider the measurement of a quantity T(x) using a linear system characterized by a response function R(x,u). The relation between the measured signal, M(u), and the true signal, T(x), may be represented as:

$$M(u) = \int_0^\infty R(x,u) * T(x) * dx + N(u) \qquad \text{Eq 1}$$

where:

N(u) = random noise inherent in the system being measured

u = variable transformed from x by the convolution

x = variable of the true signal.

When systems exhibit translational invariance, the response function takes the form R(x − u) and Equation 1 becomes:

$$M(u) = \int_0^\infty R(x-u) * T(x) * dx + N(u) \qquad \text{Eq 2}$$

Equations 1 and 2 are commonly referred to as the *convolution integral* (12).

For discrete spectra, such as the gamma-ray interrogation spectrum considered here, the random noise N(u) can be suppressed to a much smaller value than the integral. Therefore, the neglect of N(u) in Equation 1 or 2 may not introduce significant error.

Obviously, the task of data analysis is to obtain the true signal, T(x), from the measured numbers of M(u). Procedures to solve Equation 2 are referred to as *deconvolutions* (13).

Problem

A PDD spectrum is a plot of the number of occurrences versus counting rates (counts/sampling time). Examples are given in Figures 1 to 5. The PDD spectrum for an unperturbed system, such as the spectrum measured in a homogeneous flow field, has a Poisson distribution which is equivalent to a Gaussian distribution when the counting rate is high:

$$Y(N) = H * \exp[-(N - C)^2 / (2 * \sigma^2)] \qquad \text{Eq 3}$$

where:

C = counting rate at the peak centre

H = peak height

N = counting rate [or alternatively, the channel number]

σ = standard deviation

Y(N) = height at counting rate N.

For a multi-phase flow, the measured PDD spectrum is, in principle, the convolution of many Poisson spectra in which the peak heights and centre positions may be different from one another. This is caused by the fact that under a given set of conditions, the bubble sizes and the shapes of individual bubbles are different. Each Gaussian sub-peak represents the fraction of time (over the sum of all the peaks) in which a particular hydrodynamic phenomenon, (e.g., local holdup) is observed. This is typical for bubble columns in which the hydrodynamic fluctuates with time. The whole PDD spectrum can be written as:

$$Y(N) = \sum_{i=1}^{m} \{H_i * \exp[-(N - C_i)^2 / (2 * \sigma_i^2)]\} \qquad \text{Eq 4}$$

where:

C_i = counting rate for the centre of the ith peak

m = number of Gaussian sub-peaks convoluting the spectrum and subscript i represents the i sub-peak.

Equation 4 is similar to an equation describing a digital recording of an ordinary nuclear spectrum (14), except that in the latter, energy or frequency characterized by the material is used for the abscissa and photon density is the ordinate.

The problem is to find an optimal number of peaks, m, which is equal to the actual number of peaks (M) and value of H_i and C_i with i = 1 to m such that values of Y(N) for N = 0 to ∞ calculated from Equation 2 are the best representation of Y(N) observed in measurements. All of these parameters are independent variables.

A comparison of Equation 4 with the generalized Equation 2 shows the following equivalences in operators and parameters between the two cases:

$x <=====> N$

$u <=====> C_i$

$M(x) <=====> Y(N)$

$T(u) <=====> H(C_i)$

$R(x,u) <=====> \exp[-(N - C_i)^2/(2 * \sigma_i 2)]$

$du <=====> 1$

$\infty <=====> \sum_i(\delta(C_i)) *$

where:

$<=====>$ = corresponds to

$\delta(C_i)$ = a unit-sampling function.

These equivalences show that Equation 4 can be cast in the generalized form of Equation 2. Therefore, we have a typical deconvolution problem.

Theoretical Description

The least-square fitting technique is one of the best methods for determining parameters when the experimental results contain deviations and this technique is used here (15).

Let us define a set of values $[H_i^F, C_i^F(N)]$ where $i = 1$ to M that represent the final least-squared parameters, where F indicates final fitted values. Similarly, O and C indicate observed and calculated values in the iteration procedures.

According to the least-square principle (15), the problem is to find $[H_i^F, C_i^F(N_i)]$ so that:

$$S = \sum_{N=0}^{\infty} [Y^O(N) - Y^F(N)]^2 = \text{minimum} \qquad \text{Eq 5}$$

The Newton-Raphson iteration method was used to solve Equation 5 (15-17). This method involves the linearization of non-linear equations, e.g., Equation 2 or 3, by the Taylor series. This particular method requires initial values of parameters for iteration. Once reasonable initial values have been estimated, in any step of iteration, the "calculated" parameters are always regenerated. The parameters during iterations are assumed to be $[H_i^C, C_i^C]$ where $i = 1$ to m and $m > M$.

The Taylor series gives:

$$Y^F(N) = Y^C(N) + \sum_{i=1}^{m} (\partial Y^C(N) / \partial \Delta H_i) * \Delta H_i + \sum_{i=1}^{m} (\partial Y^C(N) / \partial \Delta C_i) * \Delta C_i + O(\Delta H_i^2, \Delta C_i^2) \qquad \text{Eq 6}$$

where:

$$\Delta C_i = C_i^F - C_i^C \qquad \text{Eq 7}$$

$$\Delta H_i = H_i^F - H_i^C \qquad \text{Eq 8}$$

$O(X)$ = sum of all terms with order higher than, or equal to, 2.

Inserting Equation 6 into Equation 5, neglecting higher-order terms, yields:

$$S = \sum_{N=0}^{\infty} [Y^O(N) - Y^C(N) - \sum_{i=1}^{m} \{\partial Y^C(N) / \partial \Delta H_i\} * \Delta H_i - \sum_{i=1}^{m} \{\partial Y^C(N) / \partial \Delta C_i\} * \Delta C_i]^2 = \text{minimum} \qquad \text{Eq 9}$$

This equation holds only when ΔH_i and ΔC_i are small. Otherwise, higher-order corrections must be made.

Conditions for Equation 9 are:

$$\partial S / \partial H_j = 0 \text{ where } j = 1 \text{ to } m \qquad \text{Eq 10}$$

and

$$\partial S / \partial C_j = 0 \text{ where } j = 1 \text{ to } m \qquad \text{Eq 11}$$

From Equation 9 to 11:

$$\partial S / \partial H_j \sim 2 * \sum_{N=0} \{[OMC(N) - \sum_{i=1} (\partial Y^C(N)/\partial \Delta H_i) * \Delta H_i - \sum_{i=1}^{m} (\partial Y^C(N)/\partial \Delta C_i) * \Delta C_i] * [\partial Y^C(N) / \partial \Delta H_j]\} = 0 \qquad \text{Eq 12}$$

$$\partial S / \partial \Delta C_j \sim 2 * \sum_{N=0}^{\infty} \{[OMC(N) - \sum_{i=1}^{m} (\partial Y^C(N) / \partial \Delta H_i^C) * \Delta H_i - \sum_{i=1}^{m} (\partial Y^C(N) / \partial \Delta C_i) * \Delta C_i] * [\partial Y^C(N) / \partial \Delta C_j]\} = 0 \qquad \text{Eq 13}$$

where:

$$OMC(N) = Y^O(N) - Y^C(N) \qquad \text{Eq 14}$$

Note that H_i^F and C_i^F are constants for $i = 1$ to M and H_i^F vanishes for $i = M + 1$ to m.

Since C_i^F and H_i^F are constants, according to Equation 7 and 8, the following relations hold:

$$\partial Y^C(N) / \partial \Delta H_i = -\partial Y^C(N) / \partial H_i^C \qquad \text{Eq 15}$$

$$\partial Y^C(N) / \partial \Delta C_i = -\partial Y^C(N) / \partial C_i^C \qquad \text{Eq 16}$$

Inserting Equations 15 and 16 into Equations 12 and 13 results in:

$$\sum_{N=0}^{\infty} \{A(N) * [\partial Y^C(N) / \partial \Delta H_j]\} = 0 \text{ for } j = 1 \text{ to } m \qquad \text{Eq 17}$$

$$\sum_{N=0}^{\infty} \{A(N) * [\partial Y^C(N) / \partial \Delta C_j]\} = 0 \text{ for } j = 1 \text{ to } m \qquad \text{Eq 18}$$

where:

$$A(N) = [OMC(N) + \sum_{i=1}^{m} \{\partial Y^C(N) / \partial \Delta H_i^C + * \Delta H_i + \sum_{i=1}^{m} \{\partial Y^C(N) / \partial \Delta C_i^C\} * \Delta C_i\}] \qquad \text{Eq 19}$$

and from Equations 3, 15, and 16:

$$\partial Y^C(N) / \partial \Delta H_i^C = \exp[-(N - C_i^C)^2 / (2 * \sigma_i^2)] \qquad \text{Eq 20}$$

$$\partial Y^C(N) / \partial \Delta C_i^C = [(N - C_i^C) * H_i / \sigma_i^2] * \exp[-(N - C_i^C)^2 / (2 * \sigma_i^2)] \qquad \text{Eq 21}$$

Equations 17 and 18 provide 2 m linear equations for 2 m unknowns, (ΔH_j,ΔC_j) with j = 1 to m. Although m > M, the iteration (see below) will eliminate the extra m − M peaks, originally assumed at the beginning of iteration.

Iteration Procedure

To solve the problem, the following procedure, based on the theory developed in the previous section, can be used:

1. Estimate a set of (H_i^C,C_i^C) values for i = 1 to m with m > M, where M is still unknown. (However, the choice of m can be easily made by the procedure described later.)
2. Calculate the σ_i for i = 1 to m, according to the calibration from experiments, or from the theory described earlier (18).
3. Calculate values of $Y^C(N)$, according to Equation 4 for the range of N observed. These allow the calculation of OMC(N) defined in Equation 14.
4. Formulate 2 m linear equations according to Equations 17 and 18 with the assistance of Equations 19 to 21.
5. Solve the 2 m linear equations to obtain the variables (ΔH_i,ΔC_i) for i = 1 to m.
6. Calculate the new parameters (H_iC,C_iC) for i = 1 to m, according to the following equations analogous to Equations 7 and 8:

$$H_i = H_i^C + \Delta H_i^C \qquad \text{Eq 22}$$

$$C_i = C_i^C + \Delta C_i^C \qquad \text{Eq 23}$$

where i = 1 to m.

These values will become closer to the final fitted values if the higher-order effects are much smaller than the first-order effects described in Equation 6.

7. Assign the new parameters for next iteration by:

$$H_i^C = H_i \qquad \text{Eq 24}$$

$$C_i^C = C_i \qquad \text{Eq 25}$$

for i = 1 to m.

8. When some of the H_i^C values become very small (indicating they are extra parameters originally assumed in the input) they are neglected.
9. Calculate the root mean squared deviation of fit, using the new parameters. If the deviation converges when compared with the results from the previous iteration, the calculation can be terminated.
10. Repeat Procedure 2 for the next iteration.

Other Applications

The deconvolution method can be used for almost any type of spectroscopy where quantized discrete spectra exist. In the deconvolution of ordinary spectra (e.g., Mossbauer spectrum) the frequencies of peak centres are fixed. Therefore, known numbers of C_i — where i = 1 to m (m > M) — can be initially assigned. The problem is then simplified to only one set of m linear equations resulting from Equation 17. This is much simpler than the case considered here.

Note that in particular applications, the appropriate response function (e.g., slit function in the optical spectroscopy, or 'kernel' in the nuclear spectroscopy equivalent to that of Equation 1) must be used.

NUMERICAL EXAMPLES

A computer program based on the procedures described above was written in Fortran-77 for a Cromemco System One computer. It has been tested to deconvolute spectra simulated by given parameters and spectra observed in two-phase flow measurements using the gamma-ray interrogation technique (10,11). Some examples are given below.

In the gamma-ray interrogation equipment, a multichannel analyzer coupled with a rate meter capable of signal suppression was used. The counting rate N is linearly proportional to the channel number. Therefore, examples of probability density distribution spectra will be expressed as number of occurrences versus channel number. Since a high counting rate system is used, the PDD spectrum for an unperturbed system is nearly a perfect Gaussian which is assumed for the response function. The instrument was calibrated using a pulse generator. It showed that the true signal was a unit-sampling function, i.e., each frequency is represented by a single channel. The standard deviation of the Gaussian peaks is given by (11):

$$\sigma_i = 19.3 + 0.00743 * (C_i - 172) \qquad \text{Eq 26}$$

This relation was used for both simulated and observed spectra.

Initial Estimation of Convoluting Peaks

A convoluted PDD spectrum has a full width at half maximum [FWHM] always larger than, or equal to, the theoretical FWHM of the unperturbed PDD spectrum at the same peak position. Also, the channel number of the peak maximum is always close to a peak in the convoluted spectrum. Based on this fact, the value of C_1^C can then be assigned to the position of peak maximum.

Using the peak height at maximum, the C_1^C, then σ_1 from Equation 26, a theoretical Gaussian peak based on Equation 1 was calculated. Subtraction of the calculated Gaussian peak from the original PDDS resulted in the first differential PDD spectrum. This method is referred to as *spectrum stripping*. Subsequently, the differential PDD spectrum from this step was considered independently for further spectrum stripping to obtain the centre position of the next peak by the same technique. This procedure was repeated until the differential spectrum became very small. Thus, m central positions were estimated for the initial iteration.

Following the spectrum stripping, the peak positions, C_i, where $i = 1$ to m, were fixed and a least-square procedure was used to obtain the initial estimated input peak heights, H_i^C, where $i = 1$ to m. Very small or negative peaks were ignored. A new number of (H_i^C, C_i^C) where $i = 1$ to a new number m′ was then obtained. We observed that the m′ was always larger than the final fitted number of peaks, M, thus fulfilling the requirement of the Newton-Raphson iteration method.

In the example given in Table 1, five peaks located at channels 194, 227, 269, 313 and 355, with heights of 2043.9, 261.2, 172.8, 143.3 and 11.03, respectively, were assumed. These values and Equation 26 were used in Equation 4 to construct the simulated spectrum. The simulated spectrum was then considered as observed data, $Y^O(N)$, for deconvolution. The first section of Table 1 lists the assumed parameters. In this case, the value of M is 5. Results of the spectrum stripping are given in the second section of Table 2. This gives a value of $m' = 7$, larger than $M = 5$.

Deconvolution of Simulated PDD Spectra

In this section, deconvolution of some simulated spectra is shown. The input peak positions and heights, as shown in Tables 2 to 6, were used to calculate the simulated PDDS based on Equation 4 and 26. The simulated PDDS were then deconvoluted by the procedures described above.

Table 1 lists the results of individual iteration steps followed by a comparison of observed and calculated values with their differences obtained in the sixth iteration.

In each iteration, following the list of root-mean-squared deviations of fit, values of H_i^C and C_i^C were listed in "List of Corrections". The new parameters C_i^C and H_i^C, obtained from Equations 23 and 22, respectively, were then listed. Although six iterations were shown here, only five iterations were needed to give a good fit.

Tables 2 to 6 summarize the results of some examples. For the PDDS convoluted from two peaks at channels 200 and 210 with heights of 1500 and 500 occurrences, respectively, only three iterations are required to obtain a satisfactory result (Table 2). Table 3 shows that a PDD spectrum consisting of a symmetrical pair of Gaussians with a centroid space of ten channels requires only about six iterations. Three observed spectra shown in Figures 1 to 3 by dots were reconstructed and then deconvoluted. Results are given in Tables 1, 4, 5 and 6. All converged quickly.

Deconvolution of Observed PDD Spectra

More than 200 PDDS measurements were recorded from hydrogen-pitch two-phase flows in a 3.81 cm ID bubble column with and without continuous liquid flow (11) and have been successfully deconvoluted by the program developed.

Figures 1 to 5 show various shapes of PDDS (dots). They were deconvoluted to obtain the peak heights and positions using the numerical method described above.

The deconvoluted spectra are shown by vertical bars. The peak centre positions and heights resulting from deconvolution were used to calculate the PDD spectra shown by solid curves for comparison with the observed spectra. All of them show excellent fit between observed and calculated data.

DISCUSSION

The problem considered is very similar to the analysis of seismic data or data in sonar or radar detections, in which deconvolution techniques are used for the interpretation of echoes due to a signal pulse of possibly unknown shape from objects of unknown position (19). Methods for dealing with this problem are commonly based on the Taylor minimizing technique (19) or the Baysian algorithm (20-23). Other methods were also used (24).

Both methods are similar to the theory described involving the formulation of recursion equations. The Baysian technique was originally formulated by the Fourier transform. Recently, Kennett et al. (20-23) formulated it by the Laplace transform method. The result of transformation forms a set of linear equations similar to Equations 17 and 18. They can be written in a recursion form to be solved by digital computer. It requires a large computer memory and a procedure to solve a large eigenvalue matrix. Therefore, for the problems considered, the present method is much more efficient.

The spectrum deconvolutions are very often used in optical spectroscopy to obtain electron, vibration, and rotational parameters as described by the so-called *spectrum contour analysis* (25). The analysis of ESCA and Mossbauer and other nuclear spectra is also identical to the optical spectral contour analysis. In these fields, the spectrum is convoluted by peaks with centres characterized by well-known formulae consisting of quantum numbers and parameters (14,26). The deconvolution method described here can be easily applied to these fields.

Finally, the neglect of the random noise term N(u) in Equation 1 can often be justified from the experimental set up. For example, as discussed in a previous report, the noise in the gamma-ray interrogation method can be suppressed sufficiently by using the narrow beam technique (10).

ACKNOWLEDGEMENTS

The author sincerely thanks D.J. Patmore and W.H. Dawson of the Energy Research Laboratories, CANMET, and J.J. Lipsett of AECL-CRNL for their interest and encouragement during the course of this work.

The author also sincerely thanks his wife, Esther, for carrying out a major part of the literature survey and to Nita Harcourt for editing the text.

REFERENCES

1. Shah, Y.T. "Bubble column: An overview"; *ACS Symp Ser* 168:203; 1981.
2. Shah, Y.T. *Gas-Liquid-Solid Reactor Design*; NY; McGraw-Hill; 1979.
3. Moo-Young, M. "Three phase reactors: Application to biological reactors"; Chapter 14 of the Lecture Notes for a course on three phase reactors given at Waterloo University; Sept. 27-Oct. 1, 1982.
4. McCabe, W.L. and Smith, J.C. *Unit Operations of Chemical Engineering*; 3rd ed.; NY; McGraw-Hill; 1976.
5. Charpentier, J.C. "Mass transfer rate in gas-liquid absorbers and reactors"; *Adv Chem Eng* 11:1; 1981.
6. Liu, D.D.S.; MacFarlane, R.; and Saltvolt, J.R. "Development of instrument for combustion studies: Part 1 — Tests of ionization probes for CTF applications"; Atomic Energy of Canada Limited; *Report* WNRE-512-1; 1981.
7. Liu, D.D.S. and MacFarlane, R. "Studies in hydrogen combustion using open burners: Part I — A Laser-Doppler anemometer and its application to burner velocity distribution measurements"; Atomic Energy of Canada Limited; *Report* WNRE-476-1; 1980.
8. Danel, F. and Delhaye, J.M. "Sonde optique pour mesure du taux de présence local en écoulement diphasique"; Mesures-Régulation-Atomatisé 99-101; août-sept. 1971.
9. Hsu, Y.Y.; Simon, F.F.; and Graham, R.W. "Application of hot-wire anemometry for two-phase flow measurements such as void fraction and slip-velocity"; Multiple Phase Flow Symp.; Lipstein, N.J.; ed.; *ASEM*: 26-34; 1963.
10. Liu, D.D.S.; Lipsett, J.J.; and Noble, R.D. "Development of gamma-ray interrogation techniques for multi-phase flow hydrodynamic studies: Part 1 — Principle and feasibility tests"; (In prep).
11. Liu, D.D.S. and Lipsett, J.J. Private communication.
12. Irving, J. and Mullineux, N. *Mathematics in Physics and Engineering*; NY; Academic Press; 1959.
13. Bracewell, R. *The Fourier Transform and its Applications*; NY; McGraw-Hill; 1965.
14. Evans, R.D. *The Atomic Nucleus*; NY; McGraw-Hill; 1955.
15. Ralston, A. *A First Course in Numerical Analysis*; NY; McGraw-Hill; 1965.
16. Carnahan, B.; Luther, H.A.; and Wilkes, J.O. *Applied Numerical Methods*; NY; John Wiley; 1969.
17. Hamming, R.W. *Numerical Methods for Scientists and Engineers*; NY; McGraw-Hill; 1962.
18. Price, W.J. *Nuclear Radiation Detection*; NY; McGraw-Hill; 1958.
19. Delves, L.M. and Samba, A. "Deconvolution of seismic data"; *Computer Phys Commun* 26:473; 1982.
20. Kennett, T.J.; Prestwich, W.V.; and Robertson, A. "Baysian deconvolution I: Convergent properties"; *Nucl Instr Methods* 151:285; 1978.
21. Kennett, T.J.; Prestwich, W.V.; and Robertson, A. "Baysian deconvolution II: Noise properties"; *Nucl Instr Methods* 151:293; 1978.
22. Kennett, T.J.; Prestwich, W.V.; and Robertson, A. "Baysian deconvolution III: Applications and algorithm implementation"; *Nucl Instr Methods* 153:125; 1978.
23. Kennett, T.J. and Prestwich, W.V. "On the deconvolution of exponential response functions"; *Phys Med Biol* 24:1107; 1979.
24. Doroshenko, J.J.; Kraitor, S.N.; Kurznetsova, T.V.; Kushnereva, K.K.; and Leonov, E.S. *Nucl Tech* 23:296; 1977.
25. Brand, J.C.D., Liu, D.D.S., Chan, H.W., Callomon, J.H. and Watson, J.K.G. "The 3820 Å system of propynal: Rotational analysis of the O-O band"; *J Mol Spectry* 50:304; 1974.
26. Herzberg, G. "Molecular spectra and molecular structure, III. Electronic spectra and electronic structure of polyatomic molecules"; Princeton, N.J.; Van Nostrand; 1967.

TABLES

Table 1 — Results from iteration calculations during deconvolution of PDDS — Example 1

```
  LIST OF INPUT DATA

  I=  1  CENTRE =  194    HEIGHT =  2043.9
  I=  2  CENTRE =  227    HEIGHT =   261.2
  I=  3  CENTRE =  269    HEIGHT =   172.8
  I=  4  CENTRE =  313    HEIGHT =   143.3
  I=  5  CENTRE =  355    HEIGHT =   110.3

INPUT DATA FOR LEAST SQUARES:  RESULTS FROM STRIPPING

I= 1 CENTRE(I) = 195.0   PEAK(I) =  2110.796
I= 2 CENTRE(I) = 241.0   PEAK(I) =   213.207
I= 3 CENTRE(I) = 309.0   PEAK(I) =   143.606
I= 4 CENTRE(I) = 353.0   PEAK(I) =   124.110
I= 5 CENTRE(I) = 275.0   PEAK(I) =   113.309
I= 6 CENTRE(I) = 223.0   PEAK(I) =    28.442
I= 7 CENTRE(I) = 381.0   PEAK(I) =     3.869

   ITERATION No. =  0

ROOT-MEAN-SQUARED DEVIATION = 12.71

I= 1 CENTRE(I) = 195.0   PEAK(I) =  2110.796
I= 2 CENTRE(I) = 241.0   PEAK(I) =   213.207
I= 3 CENTRE(I) = 309.0   PEAK(I) =   143.606
I= 4 CENTRE(I) = 353.0   PEAK(I) =   124.110
I= 5 CENTRE(I) = 275.0   PEAK(I) =   113.309
I= 6 CENTRE(I) = 223.0   PEAK(I) =    28.442
I= 7 CENTRE(I) = 381.0   PEAK(I) =     3.869

LIST OF CORRECTIONS

    1  delta-Height = -.7479E+02  delta-Centre = -.1022E+01
    2  delta-Height = -.1776E+03  delta-Centre =  .8925E+00
    3  delta-Height = -.3078E+01  delta-Centre =  .3956E+01
    4  delta-Height = -.1443E+02  delta-Centre =  .1164E+01
    5  delta-Height =  .4543E+02  delta-Centre = -.6555E+01
    6  delta-Height =  .2194E+03  delta-Centre =  .2128E+02
    7  delta-Height = -.1312E+01  delta-Centre = -.6837E+01
```

Table 1 (continued)

```
   ITERATION No. =  1


ROOT-MEAN-SQUARED DEVIATION = 35.26

I= 1 CENTRE(I) = 194.0   PEAK(I) =  2036.002
I= 2 CENTRE(I) = 241.9   PEAK(I) =    35.613
I= 3 CENTRE(I) = 313.0   PEAK(I) =   140.528
I= 4 CENTRE(I) = 354.2   PEAK(I) =   109.676
I= 5 CENTRE(I) = 268.4   PEAK(I) =   158.740
I= 6 CENTRE(I) = 233.0   PEAK(I) =   247.839
I= 7 CENTRE(I) = 374.2   PEAK(I) =     2.557


LIST OF CORRECTIONS

    1  delta-Height =  .1034E+02  delta-Centre =  .9690E+00
    2  delta-Height = -.1573E+03  delta-Centre =  .7694E+02
    3  delta-Height =  .1329E+01  delta-Centre =  .1905E+01
    4  delta-Height =  .5731E+01  delta-Centre =  .2278E+01
    5  delta-Height = -.3166E+02  delta-Centre =  .4990E+01
    6  delta-Height =  .1920E+03  delta-Centre = -.8214E+01
    7  delta-Height = -.1030E+02  delta-Centre =  .2526E+02


   ITERATION No. =  2


ROOT MEAN SQUARED DEVIATION = 57.55

I= 1 CENTRE(I) = 194.9   PEAK(I) =  2046.347
I= 2 CENTRE(I) = 314.9   PEAK(I) =   141.857
I= 3 CENTRE(I) = 356.4   PEAK(I) =   115.408
I= 4 CENTRE(I) = 273.4   PEAK(I) =   127.085
I= 5 CENTRE(I) = 224.8   PEAK(I) =   439.851


LIST OF CORRECTIONS

    1  delta-Height =  .9845E+01  delta-Centre =  .7913E-01
    2  delta-Height =  .3688E+01  delta-Centre = -.1516E+01
    3  delta-Height = -.4294E+01  delta-Centre = -.1023E+01
    4  delta-Height =  .4027E+02  delta-Centre = -.5793E+01
    5  delta-Height = -.1859E+03  delta-Centre =  .2454E+01
```

Table 1 (continued)

```
   ITERATION No. =  3


ROOT-MEAN-SQUARED DEVIATION = 23.84

I= 1 CENTRE(I) = 195.0   PEAK(I) =  2056.192
I= 2 CENTRE(I) = 313.3   PEAK(I) =   145.545
I= 3 CENTRE(I) = 355.4   PEAK(I) =   111.114
I= 4 CENTRE(I) = 267.6   PEAK(I) =   167.350
I= 5 CENTRE(I) = 227.2   PEAK(I) =   253.958


LIST OF CORRECTIONS

    1  delta-Height = -.2172E+02  delta-Centre = -.1056E+01
    2  delta-Height = -.2019E+01  delta-Centre = -.7133E-01
    3  delta-Height = -.6107E+00  delta-Centre = -.2761E-01
    4  delta-Height =  .6264E+01  delta-Centre =  .1846E+01
    5  delta-Height =  .1754E+02  delta-Centre = -.6968E+00


   ITERATION No. =  4


ROOT-MEAN-SQUARED DEVIATION = 21.46

I= 1 CENTRE(I) = 194.0   PEAK(I) =  2034.476
I= 2 CENTRE(I) = 313.3   PEAK(I) =   143.526
I= 3 CENTRE(I) = 355.4   PEAK(I) =   110.503
I= 4 CENTRE(I) = 269.5   PEAK(I) =   173.615
I= 5 CENTRE(I) = 226.5   PEAK(I) =   271.502


LIST OF CORRECTIONS

    1  delta-Height =  .1132E+02  delta-Centre =  .9720E+00
    2  delta-Height =  .1712E-01  delta-Centre = -.1111E+00
    3  delta-Height =  .5857E-01  delta-Centre = -.4421E-01
    4  delta-Height = -.4311E+00  delta-Centre = -.1702E+00
    5  delta-Height = -.1075E+02  delta-Centre =  .8260E+00
```

Table 1 (continued)

```
   ITERATION No. =  5

ROOT-MEAN-SQUARED DEVIATION =  .72

I= 1 CENTRE(I) = 194.9   PEAK(I) =  2045.792
I= 2 CENTRE(I) = 313.2   PEAK(I) =   143.544
I= 3 CENTRE(I) = 355.3   PEAK(I) =   110.562
I= 4 CENTRE(I) = 269.3   PEAK(I) =   173.183
I= 5 CENTRE(I) = 227.4   PEAK(I) =   260.751

LIST OF CORRECTIONS

    1  delta-Height = -.8596E+00  delta-Centre =  .1453E-01
    2  delta-Height = -.3724E+00  delta-Centre =  .3662E-01
    3  delta-Height = -.2921E+00  delta-Centre =  .1242E-01
    4  delta-Height = -.6223E+00  delta-Centre =  .7155E-01
    5  delta-Height = -.7615E+00  delta-Centre =  .1290E+00

THIS IS ITERATION =  6

ROOT-MEAN-SQUARED DEVIATION =  .43

I= 1 CENTRE(I) = 195.0   PEAK(I) =  2044.932
I= 2 CENTRE(I) = 313.2   PEAK(I) =   143.171
I= 3 CENTRE(I) = 355.4   PEAK(I) =   110.270
I= 4 CENTRE(I) = 269.4   PEAK(I) =   172.561
I= 5 CENTRE(I) = 227.5   PEAK(I) =   259.989

LIST OF CORRECTIONS

    1  delta-Height = -.3423E-02  delta-Centre =  .1459E-01
    2  delta-Height = -.1329E-01  delta-Centre =  .3754E-01
    3  delta-Height = -.9865E-02  delta-Centre =  .1191E-01
    4  delta-Height = -.1732E-01  delta-Centre =  .7250E-01
    5  delta-Height = -.2517E-01  delta-Centre =  .1299E+00
```

Table 1 (continued)

ITERATION No. = 7 (Results of the sixth iteration)

CH#	OBS	CALC	O-C
109	.15	.15	.00
110	.18	.19	.00
111	.23	.23	.00
112	.29	.29	.00
113	.35	.36	.00
114	.44	.44	.00
115	.54	.54	.00
116	.67	.67	.00
117	.82	.82	-.01
118	1.00	1.01	-.01
119	1.22	1.23	-.01
120	1.48	1.49	-.01
121	1.80	1.81	-.01
122	2.18	2.19	-.01
123	2.64	2.65	-.01
124	3.18	3.19	-.02
125	3.81	3.83	-.02
126	4.57	4.59	-.02
127	5.46	5.49	-.03
128	6.51	6.54	-.03
129	7.74	7.78	-.04
130	9.18	9.22	-.04
131	10.85	10.90	-.05
132	12.80	12.85	-.05
133	15.05	15.12	-.06
134	17.66	17.73	-.07
135	20.66	20.74	-.08
136	24.11	24.21	-.09
137	28.07	28.17	-.10
138	32.58	32.70	-.12
139	37.73	37.86	-.13
140	43.56	43.71	-.15
141	50.17	50.34	-.16
142	57.63	57.82	-.18
143	66.03	66.23	-.20
144	75.45	75.67	-.22
145	85.98	86.23	-.25
146	97.73	98.00	-.27
147	110.79	111.09	-.30
148	125.27	125.59	-.32
149	141.26	141.61	-.35
150	158.88	159.26	-.38

Table 1 (continued)

CH#	OBS	CALC	O-C
151	178.22	178.64	-.42
152	199.40	199.84	-.45
153	222.50	222.98	-.48
154	247.63	248.14	-.52
155	274.87	275.42	-.55
156	304.30	304.89	-.59
157	336.00	336.63	-.62
158	370.03	370.69	-.66
159	406.44	407.14	-.70
160	445.25	445.99	-.73
161	486.50	487.27	-.77
162	530.17	530.97	-.80
163	576.25	577.08	-.84
164	624.68	625.55	-.87
165	675.42	676.32	-.90
166	728.37	729.30	-.93
167	783.41	784.37	-.96
168	840.41	841.40	-.98
169	899.21	900.21	-1.01
170	959.60	960.63	-1.03
171	1021.38	1022.43	-1.04
172	1084.31	1085.37	-1.06
173	1148.12	1149.19	-1.07
174	1212.53	1213.61	-1.08
175	1277.22	1278.31	-1.09
176	1341.88	1342.97	-1.09
177	1406.17	1407.26	-1.09
178	1469.72	1470.81	-1.09
179	1532.19	1533.27	-1.08
180	1593.20	1594.27	-1.07
181	1652.38	1653.45	-1.06
182	1709.38	1710.43	-1.05
183	1763.81	1764.85	-1.04
184	1815.34	1816.36	-1.02
185	1863.63	1864.63	-1.00
186	1908.35	1909.33	-.98
187	1949.21	1950.17	-.96
188	1985.94	1986.88	-.94
189	2018.30	2019.22	-.92
190	2046.07	2046.96	-.89
191	2069.08	2069.95	-.87
192	2087.18	2088.03	-.85
193	2100.29	2101.11	-.82
194	2108.32	2109.12	-.79
195	2111.27	2112.04	-.77

Table 1 (continued)

CH#	OBS	CALC	O-C
196	2109.15	2109.89	-.74
197	2102.01	2102.73	-.72
198	2089.96	2090.65	-.69
199	2073.13	2073.79	-.66
200	2051.69	2052.32	-.63
201	2025.83	2026.43	-.60
202	1995.80	1996.37	-.57
203	1961.85	1962.39	-.54
204	1924.26	1924.76	-.50
205	1883.34	1883.81	-.47
206	1839.40	1839.83	-.43
207	1792.77	1793.17	-.39
208	1743.80	1744.15	-.36
209	1692.82	1693.14	-.31
210	1640.18	1640.45	-.27
211	1586.21	1586.44	-.23
212	1531.26	1531.44	-.18
213	1475.63	1475.77	-.14
214	1419.64	1419.73	-.09
215	1363.60	1363.63	-.04
216	1307.76	1307.75	.01
217	1252.39	1252.33	.06
218	1197.74	1197.62	.11
219	1144.00	1143.84	.16
220	1091.39	1091.17	.21
221	1040.06	1039.79	.26
222	990.17	989.85	.31
223	941.84	941.48	.36
224	895.18	894.77	.41
225	850.27	849.82	.45
226	807.18	806.69	.49
227	765.95	765.42	.53
228	726.61	726.04	.57
229	689.18	688.58	.60
230	653.66	653.02	.64
231	620.03	619.36	.66
232	588.26	587.58	.69
233	558.34	557.63	.71
234	530.21	529.48	.73
235	503.82	503.08	.74
236	479.13	478.38	.75
237	456.08	455.32	.76
238	434.60	433.84	.77
239	414.64	413.87	.77
240	396.12	395.35	.77

Table 1 (continued)

CH#	OBS	CALC	O-C
241	378.99	378.22	.77
242	363.17	362.41	.76
243	348.60	347.85	.75
244	335.22	334.47	.75
245	322.95	322.22	.73
246	311.74	311.01	.72
247	301.51	300.80	.71
248	292.22	291.52	.69
249	283.79	283.11	.68
250	276.16	275.50	.66
251	269.28	268.64	.65
252	263.09	262.46	.63
253	257.54	256.92	.61
254	252.56	251.96	.60
255	248.10	247.52	.58
256	244.11	243.54	.57
257	240.54	239.99	.55
258	237.34	236.81	.54
259	234.47	233.94	.52
260	231.87	231.36	.51
261	229.51	229.01	.49
262	227.34	226.86	.48
263	225.33	224.87	.47
264	223.45	222.99	.46
265	221.66	221.21	.44
266	219.93	219.49	.43
267	218.23	217.81	.42
268	216.56	216.15	.41
269	214.88	214.48	.40
270	213.19	212.80	.39
271	211.46	211.08	.38
272	209.70	209.33	.37
273	207.90	207.54	.36
274	206.06	205.71	.35
275	204.18	203.84	.34
276	202.26	201.93	.33
277	200.31	199.99	.32
278	198.34	198.03	.31
279	196.36	196.06	.30
280	194.39	194.09	.30
281	192.42	192.14	.29
282	190.49	190.21	.28
283	188.60	188.33	.27
284	186.77	186.51	.26
285	185.01	184.76	.25

Table 1 (continued)

CH#	OBS	CALC	O-C
286	183.34	183.10	.25
287	181.77	181.53	.24
288	180.30	180.07	.23
289	178.95	178.73	.22
290	177.72	177.51	.22
291	176.63	176.42	.21
292	175.66	175.46	.20
293	174.84	174.64	.20
294	174.14	173.95	.19
295	173.57	173.38	.19
296	173.13	172.95	.19
297	172.81	172.63	.18
298	172.59	172.41	.18
299	172.46	172.29	.17
300	172.42	172.25	.17
301	172.45	172.28	.17
302	172.54	172.37	.17
303	172.66	172.49	.16
304	172.80	172.64	.16
305	172.96	172.80	.16
306	173.10	172.94	.16
307	173.22	173.06	.16
308	173.30	173.15	.16
309	173.33	173.18	.15
310	173.30	173.15	.15
311	173.20	173.04	.15
312	173.01	172.86	.15
313	172.73	172.58	.15
314	172.36	172.21	.15
315	171.88	171.74	.15
316	171.31	171.17	.14
317	170.64	170.50	.14
318	169.88	169.74	.14
319	169.02	168.88	.14
320	168.07	167.94	.14
321	167.05	166.91	.13
322	165.95	165.82	.13
323	164.79	164.66	.13
324	163.58	163.45	.13
325	162.32	162.20	.13
326	161.04	160.91	.12
327	159.73	159.61	.12
328	158.42	158.30	.12
329	157.10	156.99	.12
330	155.80	155.69	.12

Table 1 (continued)

CH#	OBS	CALC	O-C
331	154.52	154.40	.11
332	153.26	153.14	.11
333	152.03	151.92	.11
334	150.84	150.73	.11
335	149.68	149.58	.11
336	148.57	148.47	.11
337	147.50	147.40	.10
338	146.47	146.37	.10
339	145.47	145.37	.10
340	144.51	144.41	.10
341	143.57	143.47	.10
342	142.64	142.54	.10
343	141.73	141.63	.10
344	140.81	140.71	.10
345	139.88	139.78	.10
346	138.92	138.83	.10
347	137.93	137.84	.10
348	136.90	136.80	.10
349	135.80	135.70	.10
350	134.63	134.54	.09
351	133.38	133.29	.09
352	132.04	131.95	.09
353	130.60	130.51	.09
354	129.05	128.96	.09
355	127.38	127.29	.09
356	125.59	125.50	.09
357	123.67	123.58	.09
358	121.61	121.53	.09
359	119.43	119.34	.08
360	117.11	117.03	.08
361	114.66	114.58	.08
362	112.08	112.00	.08
363	109.37	109.30	.08
364	106.55	106.48	.07
365	103.61	103.54	.07
366	100.58	100.51	.07
367	97.45	97.38	.06
368	94.24	94.17	.06
369	90.95	90.89	.06
370	87.61	87.55	.06
371	84.22	84.16	.05
372	80.79	80.74	.05
373	77.35	77.30	.05
374	73.89	73.85	.04
375	70.44	70.40	.04

Table 1 (continued)

CH#	OBS	CALC	O-C
376	67.01	66.97	.04
377	63.61	63.57	.04
378	60.25	60.21	.03
379	56.94	56.91	.03
380	53.69	53.66	.03
381	50.52	50.49	.03
382	47.43	47.41	.02
383	44.43	44.41	.02
384	41.52	41.50	.02
385	38.72	38.70	.02
386	36.02	36.01	.02
387	33.44	33.43	.01
388	30.97	30.96	.01
389	28.62	28.61	.01
390	26.38	26.38	.01
391	24.27	24.26	.01
392	22.27	22.26	.01
393	20.39	20.39	.01
394	18.63	18.62	.00
395	16.98	16.97	.00
396	15.43	15.43	.00
397	14.00	14.00	.00
398	12.67	12.67	.00
399	11.44	11.44	.00
400	10.31	10.31	.00
401	9.26	9.26	.00
402	8.31	8.31	.00
403	7.43	7.43	.00
404	6.63	6.63	.00
405	5.91	5.91	.00
406	5.25	5.25	.00
407	4.65	4.65	.00
408	4.11	4.11	.00
409	3.63	3.63	.00
410	3.19	3.19	.00
411	2.80	2.80	.00
412	2.45	2.46	.00
413	2.15	2.15	.00
414	1.87	1.87	.00
415	1.63	1.63	.00
416	1.41	1.41	.00
417	1.22	1.22	.00
418	1.06	1.06	.00
419	.91	.91	.00
420	.78	.78	.00

Table 1 (continued)

CH#	OBS	CALC	O-C
421	.67	.67	.00
422	.57	.57	.00
423	.49	.49	.00
424	.42	.42	.00
425	.35	.35	.00
426	.30	.30	.00
427	.25	.25	.00
428	.21	.21	.00
429	.18	.18	.00
430	.15	.15	.00
431	.13	.13	.00
432	.11	.11	.00
433	.09	.09	.00
434	.07	.07	.00
435	.06	.06	.00
436	.05	.05	.00
437	.04	.04	.00
438	.03	.03	.00

ROOT MEAN SQUARED DEVIATION = .44

THE FINAL RESULTS

I= 1 CENTRE(I) = 195.0 PEAK(I) = 2044.929
I= 2 CENTRE(I) = 313.2 PEAK(I) = 143.158
I= 3 CENTRE(I) = 355.4 PEAK(I) = 110.260
I= 4 CENTRE(I) = 269.5 PEAK(I) = 172.544
I= 5 CENTRE(I) = 227.6 PEAK(I) = 259.964

Table 2 — Results of iterations during PDDS deconvolution — Example 1

Peak	1		2		3		4		5		RMS
	CN#	Peak	CH#	Peak	CH#	Peak	CH#	Peak	CH#	Peak	Deviation
Input	194.0	2043.9	227.0	261.2	269.0	172.8	313.0	143.3	355.0	110.3	
After Spectrum stripping	195.0	2110.8	241.0 223.0	213.2 28.4	275.0	113.3	309.0	143.6	353.0 381.0	124.1 3.9	12.71
After 1st Iteration	194.0	2036.0	241.9 233.0	35.6 247.8	268.4	158.7	313.0	140.5	354.2 374.2	109.7 2.6	35.26
After 2nd Iteration	194.9	2046.3	224.8	439.9	273.4	127.1	314.9	141.9	356.4	115.4	57.55
After 3rd Iteration	195.0	2056.2	227.2	254.0	267.6	167.4	313.3	145.5	355.4	111.1	23.84
After 4th Iteration	194.0	2034.5	226.5	271.5	269.5	173.6	313.3	143.5	355.4	110.5	21.46
After 5th Iteration	194.9	2045.8	227.4	260.8	269.3	173.2	313.2	143.5	355.4	110.6	0.72
After 6th Iteration	195.0	2044.9	227.5	260.0	269.3	172.6	313.2	143.17	355.4	110.3	0.43

Table 3 — Results of iterations during PDDS deconvolution — Example 2

Peak	1		2		RMS Deviation
	CH#	Peak	CH#	Peak	
Input data	200.0	1500.0	210.0	500.0	
After spectrum stripping	202.0	1943.5	230.0	53.9	6.85
After 1st iteration	201.4	1882.0	220.0	113.8	17.11
After 2nd iteration	201.2	1742.4	210.0	258.6	13.54
After 3rd iteration	200.3	1508.6	211.3	497.0	6.91
After 4th iteration	200.4	1538.2	210.8	461.7	5.91
After 5th iteration	200.4	1486.5	210.6	513.0	2.05
After 6th iteration	200.4	1508.8	210.6	490.9	1.38
After 7th iteration	200.4	1500.1	210.6	499.5	0.13

Table 4 — Results of iterations during PDDS deconvolution — Example 3

Peak	1		2		RMS Deviation
	CH#	Peak	CH#	Peak	
Input data	200.0	1500.0	210.0	1500.0	
After Spectrum Stripping	204.0	2855.3	231.0	151.7	16.56
After 1st iteration	203.5	2725.9	221.0	264.2	30.12
After 2nd iteration	202.7	2318.1	211.0	685.0	47.25
After 3rd iteration	201.0	1854.5	209.8	1055.8	58.54
After 4th iteration	200.5	1622.2	211.6	1378.8	7.16
After 5th iteration	200.7	1553.9	210.8	1444.7	8.34
After 6th iteration	200.6	1478.8	210.7	1520.2	3.17
After 7th iteration	200.7	1510.0	210.7	1489.3	1.60
After 8th iteration	200.7	1497.7	210.7	1501.6	0.40

Table 5 — Results of iterations during PDDS deconvolution — Example 4

Peak	1		2		3		4		RMS Deviation
	CN#	Peak	CH#	Peak	CH#	Peak	CH#	Peak	
Input	189.0	1523.9	219.0	781.6	255.0	335.6	289.0	73.4	
After Spectrum stripping	195.0	1858.3	236.0	598.3	274.0	189.5	311.0	11.3	55.69
After 1st Iteration	190.7	1643.1	226.0	605.6	264.0	316.2	301.0	119.7	70.18
After 2nd Iteration	190.1	1568.1	218.6	742.8	255.2	323.2	294.6	75.2	27.21
After 3rd Iteration	189.1	1516.0	219.5	793.7	255.6	337.4	291.3	68.0	4.32
After 4th Iteration	189.1	1524.8	219.6	781.4	255.7	355.9	289.4	72.2	0.50
After 5th Iteration	189.1	1523.8	219.6	781.6	255.7	335.5	289.4	73.3	0.03
After 6th Iteration	189.1	1523.8	219.6	781.6	255.7	355.5	289.4	73.4	0.04

Table 6 — Results of iterations during PDDS deconvolution — Example 5

Peak	1		2		RMS Deviation
	CH#	Peak	CH#	Peak	
Input	171.0	2753.0	203.0	27.6	
After spectrum stripping	171.0	2754.7	205.0	26.9	0.63
After 1st iteration	171.0	2753.2	203.1	27.4	0.09
After 2nd iteration	171.0	2753.0	203.1	27.6	0.00
After 3rd iteration	171.0	2753.0	203.1	27.6	0.00

FIGURES

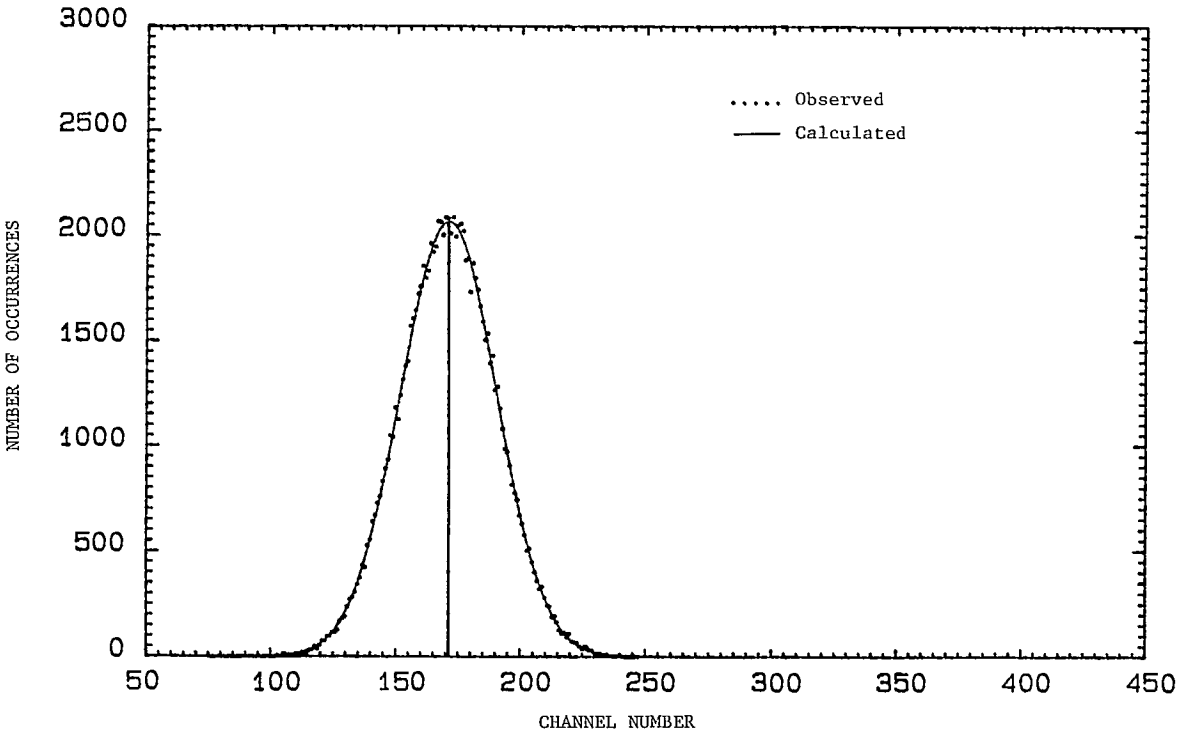

Fig. 1 – Observed and calculated PDD spectrum for Run 84-FD-946 at temperature of 200°C, pressure of 2.76 MPa and superficial gas velocity of 0.00 cm/s

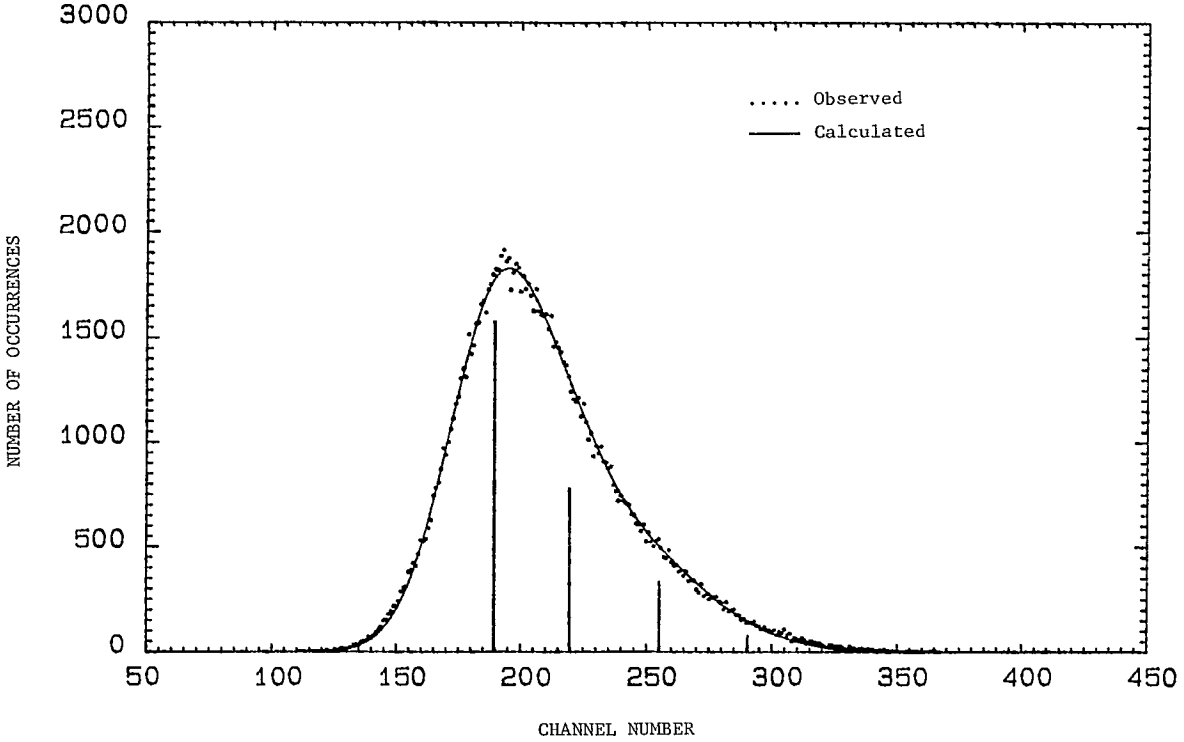

Fig. 2 – Observed and calculated PDD spectrum for Run 84-FD-615 at temperature of 200°C, pressure of 13.79 MPa and superficial gas velocity of 1.77 cm/s

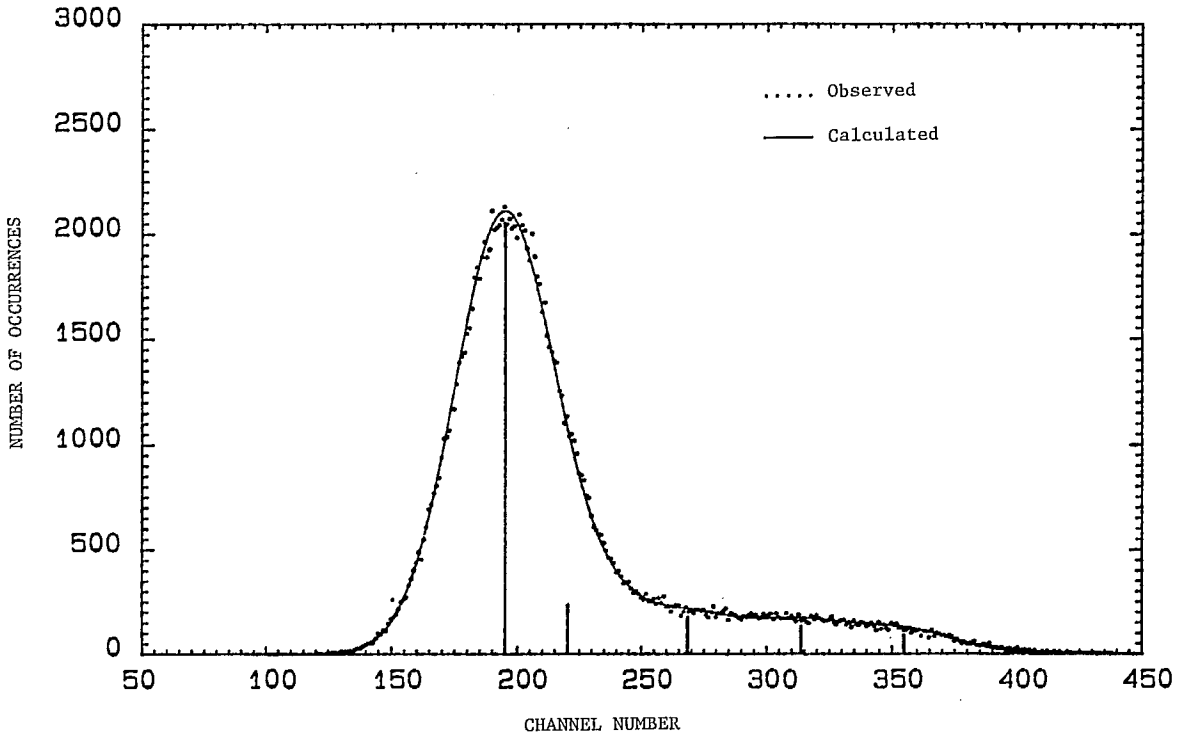

Fig. 3 – Observed and calculated PDD spectrum for Run 84-FD-657 at temperature of 200°C, pressure of 13.79 MPa and superficial gas velocity of 1.31 cm/s

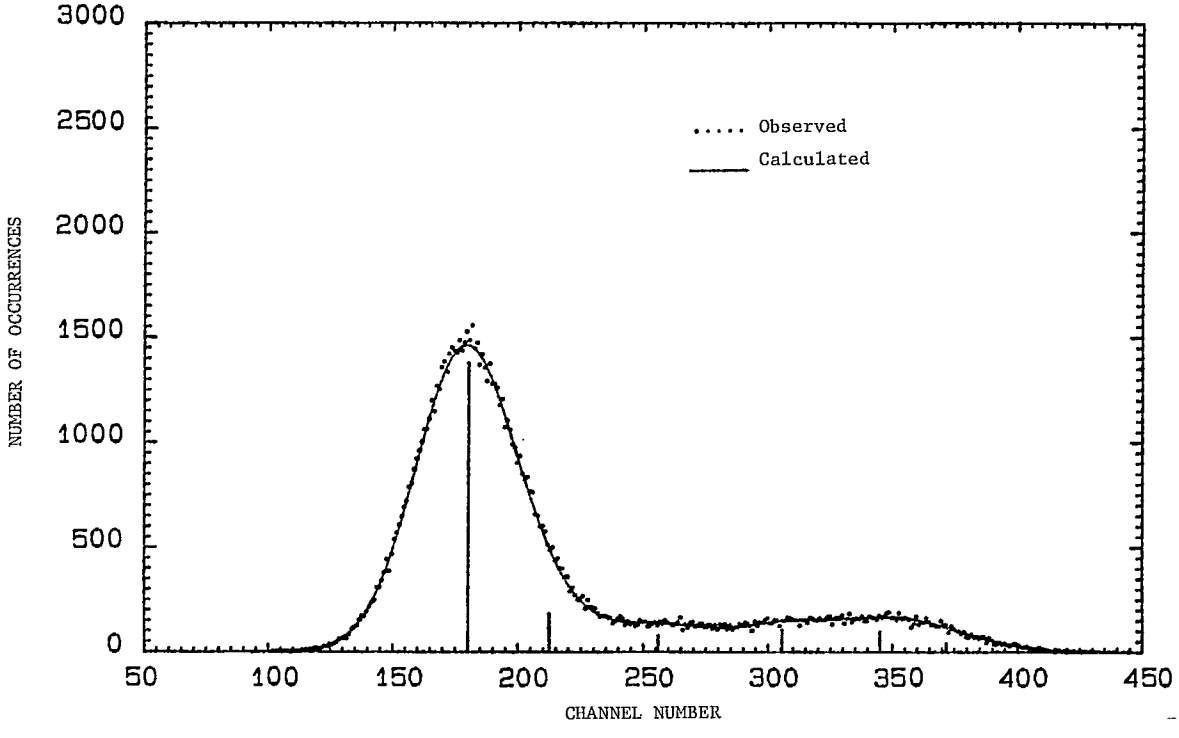

Fig. 4 – Observed and calculated PDD spectrum for Run 84-FD-990 at temperature of 200°C, pressure of 2.76 MPa and superficial gas velocity of 2.38 cm/s

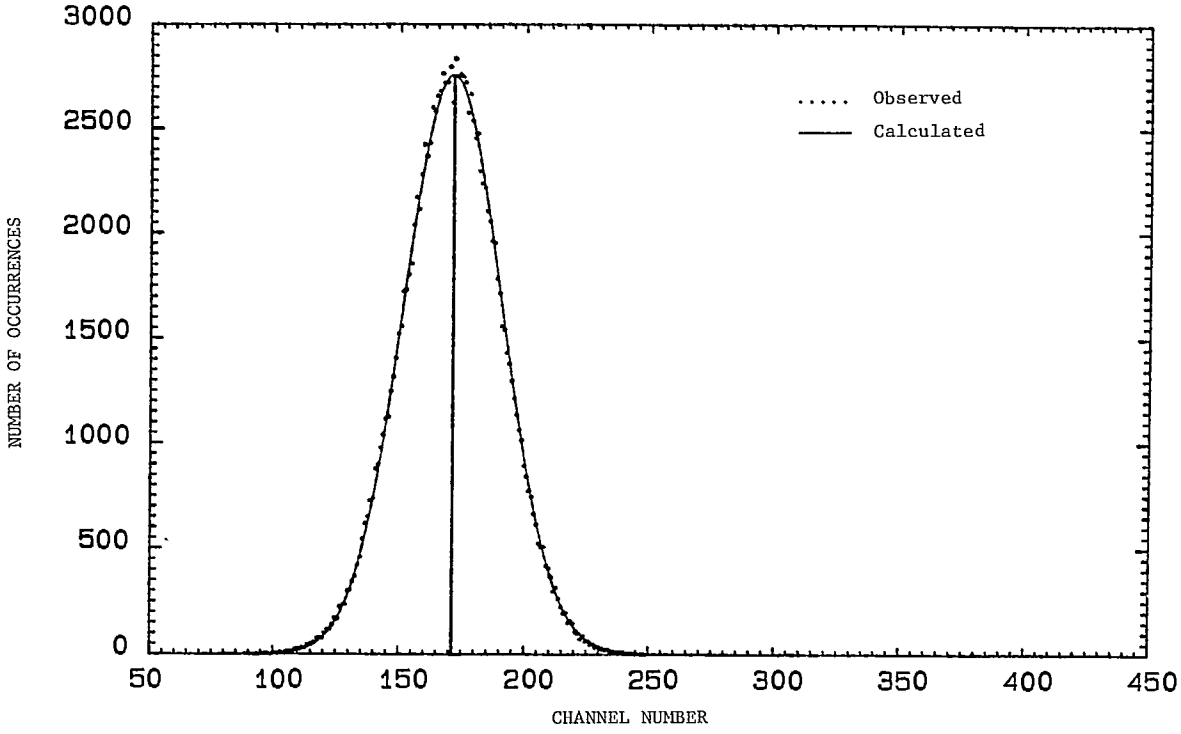

Fig. 5 – Observed and calculated PDD spectrum for Run 84-FD-681 at temperature of 200°C, pressure of 13.79 MPa and superficial gas velocity of 0.53 cm/s